Journal of Advanced Engineering Trends

ISSN : 2682 - 2091

Vol.43, No.1. January 2024

http://jaet.journals.ekb.eg

Dynamic Performance Analysis of An Electric Vehicle System Using Different Control Algorithms

Mohamed R. M. Hassan[1 *], Mahmoud A. Mossa[1] and Gamal M. Dousoky[1]

Electrical Engineering Department, Faculty of Engineering, Minia University, Egypt[(1, 1*)]

* Corresponding author: *mohamed.hassan@mu.edu.eg*

ARTICLE INFO

Article history:
Received:
Accepted:
Online:

Keywords:
Electric Vehicle (EV)
IM drive
FOC
MP-DTC
PCC
Dynamic analysis

ABSTRACT

This study introduces a comprehensive dynamic performance analysis of an electric vehicle (EV) system using different control techniques in order to define the most effective control technique for induction motor (IM) in an EV system. The entire EV system components are initially modeled in detail. The electric vehicle system dynamic is then tested using three different controllers: field-oriented control (FOC), model predictive direct torque control (MP-DTC),and finite control set predictive current control (FCS-PCC) techniques. The implementation of the FOC is based on a hysteresis current controller (HCC) which forces the input current of the IM to follow the reference current. The MP-DTC implementation is standing on a cost function which consists of the absolute errors of both the torque and flux with a weighting factor. Meanwhile, the operation of the PCC scheme articulates on a designed cost function that guarantees the minimum error between the predicted and reference currents. The EV system dynamic performance is tested by simulation using MATLAB/Simulink software. The obtained results illustrated that the electrical and mechanical dynamics of the vehicle under the PCC technique exhibit better performance compared to the results obtained using the other two control techniques. This is illustrated through the fast-dynamic response, low torque and flux ripples, and low current harmonics.

1. Introduction

Electric Vehicles (EVs) promise a good solution for green transportation needs due to their environmental and economic benefits. The main advantages of electric vehicles are well known: EVs do not pollute the air, by themselves, the driving noise is low and the efficiency is good. Also, EVs reduce petroleum consumption [1].

The main components of an EV system are the battery pack, the electric motor, the motor's controller, and the battery charger. DC motor, induction motor (IM), switched reluctance (SR) motor and brushless permanent magnet motor are the four common electric motors used in EV design[2]. The IM performance had been investigated in terms of automotive standards in EV as the best candidate for EV [3].

Many controls techniques concern with both the IM and the EV battery. A three-phase four leg inverter based on a virtual impedance coordination was presented in [4] in order to be used as an interface between the EVs and the distribution grid. References [5, 6] present two different control methods to improve the performance of the charging system of an EV.

Several control techniques were put forward for IM. In [2] a new control technique was proposed to control the IM by limiting the control cycle of both the flux and torque to obtain high efficiency and fast response. Reducing the ripple contents of both the motor's torque and flux was obtained by the model prediction direct torque control illustrated in [7]. Reference [8] illustrated three different control techniques for EV: direct torque control (DTC), field-oriented control (FOC), and space vector modulation-based DTC. An improved switching table-based DTC technique was presented in [9] to improve the IM performance.

For enhancing the dynamic performance of IM drives used for EV, vector control techniques are preferred. However, they require a complicated coordinate transformation to separate the interaction between the torque and flux controllers[10]. A vector control scheme based on indirect rotor flux orientation for induction motor in EV system was presented in [11]. A new FOC technique that applied a slip frequency control to an IM in an EV system to eliminate the effect of the parametric variation of IM was illustrated in [12]. A hysteresis band current controller based on the FOC principle was introduced in [13] to control an IM through a direct matrix converter.

Model predictive control (MPC) is used to control the electric drives and electric converters. New predictive techniques based on phase angle control and flux control were proposed in [14] and [15] respectively to enhance the IM dynamic performance. Reference [16] reported different prediction techniques that were applied to double-fed induction generators (DFIG) such as model predictive current and predictive voltage techniques. In [17, 18], the predictive current was applied to control a five-phase IM. Also, an effective model predictive current control technique was proposed to control a Sensorless IM as illustrated in [19]. An explicit control technique based on prediction voltage to control the IM as illustrated in [20] [21]. A robust predictive current control based on torque angle. In order to eliminate the torque ripple of the permanent magnet synchronous motor used in EV, [22] proposed a predictive current control technique that used a finite control set for current control. The EV dynamic performance was evaluated under three different control techniques: DTC, the model-based predictive direct torque control (MP-DTC), and the predictive voltage control (PVC) as illustrated in [23].

Revised:15 June, 2022, Accepted:3 August , 2022

In this article, the FOC based on a hysteresis current control will be developed to control the EV speed and study the vehicle dynamics. Then, the MP-DTC will be presented as a modern control technique in order to study the EV system dynamics. Also, from previous studies, the PCC technique was used to control the EV battery charging, and the torque of the PMSM of an EV but has not been applied yet to control the complete EV system driven by IM. Therefore, this article intends to develop the PCC to the IM in a complete EV system and analyses the EV electrical and mechanical dynamic performance.

The current article's contribution can be summaries as follows:

- The theoretical base of the FOC-HCC, MP-DTC and the PCC used in the EV system is presented in detail.
- The paper analyses the electrical and mechanical dynamic performance of the EV system under both the FOC-HCC and the PCC control techniques.
- A detailed comparative study of the EV performance under each of the control techniques to identify the best suitable control technique for the IM drive of the EV system.

This article is divided into five sections. Section (II) illustrates the modeling of the complete EV system elements. Section (III) discusses the control methods applied to the EV system. Section (IV) shows the test results of the EV system under FOC-HCC and PCC in addition to a comparative study of the applied techniques. Finally, section (V) concludes the study outcome.

2. Modeling of the EV system

The EV system's complete dynamic modeling is important to study both the electric and mechanical dynamic performances of an EV. The typical EV system comprises mainly the vehicle dynamics, the induction motor, the IM drive voltage source inverter (VSI), the EV battery stack as a power supply, and the transducers and sensors of the EV system. In this section, the vehicle dynamics, IM model, and battery stack model will be presented as follows:

2.1. Vehicle Dynamic Model

Based on the vehicle dynamic principles presented in [24, 25], the forces act on a moving vehicle are the uphill gravity force (F_g), the road rolling resistance force (F_{roll}), the bearing fraction force (F_{bear}), the drag force due to the aerodynamics (F_{drag}) and the required acceleration force (F_{accel}). The total force of the vehicle is called the tractive force (F_t). The tractive force of a vehicle of mass (m_v) moves with a linear velocity of (v) up a hill with a slope angle (α) is expressed as follows:

$$\begin{aligned} F_t &= F_g + F_{roll} + F_{bear} + F_{drag} + F_{accel} \\ &= \underbrace{m_v g \sin(\alpha)}_{Gravity\ force} + \underbrace{\mu_{rr} m_v g}_{Rolling\ force} + \underbrace{\frac{K_b}{r} w}_{Bearing\ force} \\ &+ \underbrace{\frac{1}{2}\rho C_d A_f (v+v_w)^2}_{Drag\ force} + \underbrace{\left(\frac{J_{ew}}{r}\right)\frac{dw}{dt}}_{Acceleration\ force} \end{aligned} \tag{1}$$

where g is the gravity acceleration, μ_{rr} is the road rolling resistance coefficient, K_b is the coefficient of bearing fraction, r is the wheel radius, w is the rotational speed of the vehicle's wheel, ρ is the air density, A_f is the front area vehicle, C_d is the aerodynamic drag coefficient, v_w is the speed of the wind on the vehicle direction of rotation, J_{ew} is the vehicle equivalent rotational inertia at the wheel and w is the vehicle wheel rotational speed.

The tractive torque required to move the EV can be given by:

$$T_t = F_t * r \tag{2}$$

The tractive torque developed by the IM of the EV (T_e) can be given by:

$$T_e = \frac{1}{\eta_G G} T_t \tag{3}$$

where G is the EV gear ratio and η_G is the efficiency gear. The vehicle wheel rotational speed can be given by:

$$\frac{dw}{dt} = \frac{r}{J_{ew}}[F_t - (F_g + F_{roll} + F_{bear} + F_{drag})] \tag{4}$$

After some manipulations, the vehicle's wheel rotational speed (4) can be replaced by the following:

$$\frac{dw_w}{dt} = \frac{1}{J_{ew}}\left[T_m \eta_G G - \left[\frac{1}{2}\rho r C_d A_f (v+v_w)^2 + r\mu_{rr} m_v g + r m_v g \sin(\alpha) + K_b w\right]\right] \tag{5}$$

2.2. Dynamic Model of Induction Motor

The squirrel cage IM per phase equivalent circuit is illustrated in Figure 1. The dynamic model of the IM in synchronous reference frame at instant KT_s is expressed by the following [26]:

The stator voltage: $$\bar{u}_{sk} = R_s \bar{\imath}_{sk} + \frac{d\bar{\psi}_{sk}}{dt} + j\omega_s \bar{\psi}_{sk} \tag{6}$$

The rotor voltage: $$0.0 = R_r \bar{\imath}_{rk} + \frac{d\bar{\psi}_{rk}}{dt} + j\omega_{slip} \bar{\psi}_{rk} \tag{7}$$

The stator flux: $$\bar{\psi}_{sk} = L_s \bar{\imath}_{sk} + L_m \bar{\imath}_{rk} \tag{8}$$

The rotor flux: $$\bar{\psi}_{rk} = L_r \bar{\imath}_{rk} + L_m \bar{\imath}_{sk} \tag{9}$$

The IM torque: $$T_{e,k} = \frac{3}{2} p \frac{l_m}{l_r} (\bar{\psi}_{dr,k} \bar{\imath}_{qs,k} - \bar{\psi}_{qr,k} \bar{\imath}_{ds,k}) \tag{10}$$

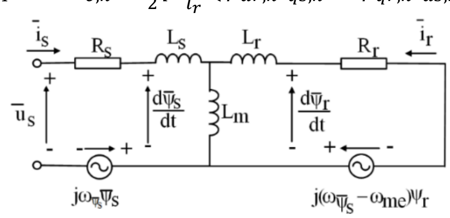

Figure 1: The IM per phase equivalent circuit

2.3. Dynamic Model of Battery Stack

The mathematical model of the EV battery during the discharging process can be expressed by a dependent voltage source matched in series with an internal resistance as presented in Figure 2. The voltage source is dependent on both the polarization voltage and the state of charge. The terminal voltage of the battery (V_{Bat}) can be expressed as the following [23]:

$$V_{Bat} = E_0 - K\frac{Q}{Q-\int i(t)dt} + Ae^{-B\int i(t)dt} - R_{int} \times i(t) \qquad (11)$$

where E_0 is the constant voltage of the EV battery(V), K is the battery polarization constant (V), Q is the capacity of the EV battery (Ah), $i(t)$ is the discharging current of the EV battery, R_{int} is the internal resistance of the EV battery, A is the exponential zone amplitude of the battery and B is the time constant inverse of the exponential zone of the EV the battery ($(Ah)^{-1}$).

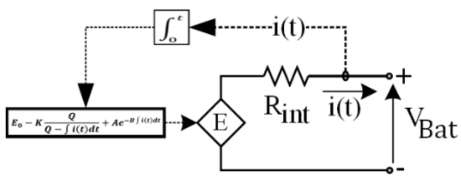

Figure 2: The EV battery equivalent circuit

3. Control Techniques

In this paper, the dynamic performance of an EV system is studied under two control techniques. The IM control techniques are the field-oriented control-based hysteresis current controller (FOC-HCC) and the finite control set predictive current control (FCS-PCC). In this section, the EV system is tested along a wide speed range using Worldwide Harmonised Light Vehicle Test Procedure (WLTP) reference. Then a comparison between the dynamic performance under both techniques is introduced to obtain the best control technique.

The measured signals used in both control techniques are the EV speed and both the stator voltages and currents. Using the measured signals, the IM torque and flux were estimated. The reference q-axis stator current component ($i^*_{qs,k}$) can be calculated using the reference torque ($T^*_{e,k}$) which is obtained through a PI closed-loop speed.

3.1. Field Oriented Control

The field-oriented control technique was developed to control the transient response of IM torque so that it acts similarly to a separately excited DC motor [27]. The FOC principle will be performed by a hysteresis current controller which is simple, fast dynamic response, and insensitive to IM parameters variation. Figure 3 illustrates the hysteresis current controller concept which consists of a comparator and hysteresis band. The main concept of this technique is to force the input current of the induction motor (IM) to follow the reference current [28]. The voltage source inverter (VSI) switching signals are generated due to the error in stator current. The error in stator current is the difference between the reference current and the actual current. In this control technique, if the stator actual current becomes more than the upper hysteresis band, the upper switch is turned off and it's complementary turned on so the stator current start to decay. On the other hand, if the stator actual current reaches the lower band of the hysteresis band, the lower switch is turned off and the upper arm is turned on to bring the current into the hysteresis band.

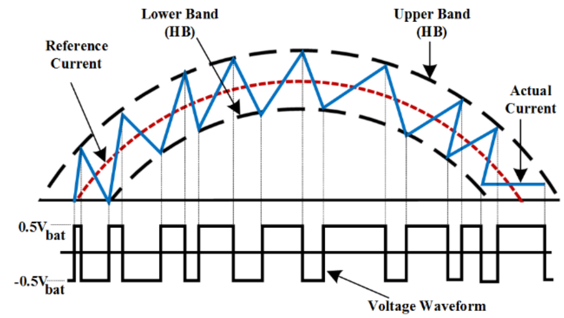

Figure 3: The hysteresis current controller concept

The FOC scheme of an IM in an EV system based on HCC is illustrated in Figure 4. FOC-HCC is used to control the vehicle speed and both the IM torque and flux. The EV speed, stator voltages, and stator currents are sensed by measuring instruments. The measured EV speed is used to calculate the reference torque through PI closed-loop control. Then, the reference torque is used in addition to reference flux to calculate the reference stator quadrature current component (i^*_{qs}). The reference flux is the nominal flux of the motor. The reference flux is used to calculate the reference stator direct component (i^*_{ds}). Based on the field orientation principles, both the references current components are expressed by the following:

$$i^*_{ds,k} = \frac{1}{l_m}\psi^*_{r\prime k} \qquad (12)$$

$$i^*_{qs,k} = \frac{2l_r}{3pl_m}\frac{T^*_{e,k}}{\psi^*_{r\prime k}} \qquad (13)$$

Then, the actual current and the reference current are fed to the hysteresis current controller to develop the inverter switching signals.

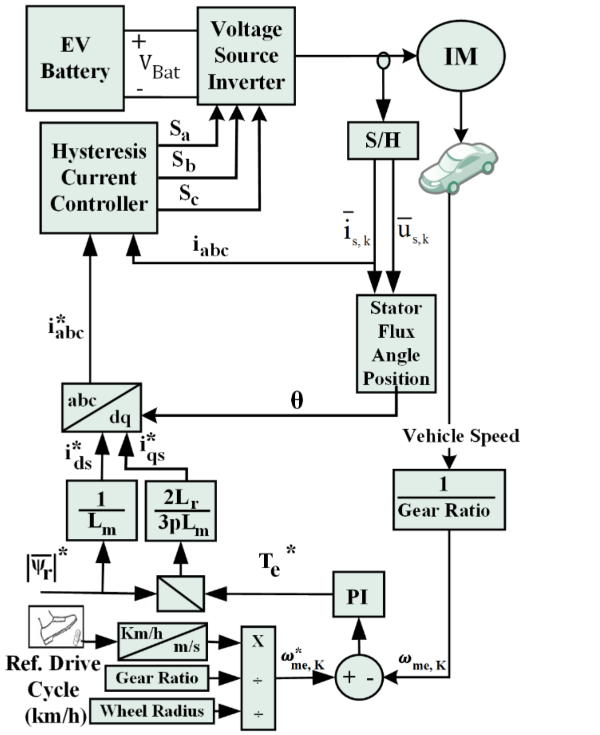

Figure 4: Block diagram of the FOC-HCC for IM in an EV system

3.2. Model Predictive Direct Torque Control

To investigate recent predictive control schemes employed by the IM, the authors in [23, 29] used a cost function which consists of the absolute error of the torque, the absolute error of the flux and a weighting factor to balance between the torque and the stator flux. The error vector can be expressed by:

$$\begin{aligned}\bar{e}_k &= \frac{Te^*_k - Te_k}{T_n} + jw_f\,\frac{|\psi^*_{s,k}| - |\bar{\psi}_{s,k}|}{\Psi_n} \\ &= e_{Te,k} + jw_f\; e_{|\bar{\psi}_s|,k}\end{aligned} \quad (14)$$

where T_n and Ψ_n are the nominal values of both the torque and flux of the IM while w_f is the weighting factor. The control target is to maintain the error vector $|\bar{e}_k|$ very close to zero, by selecting the proper voltage vector to be applied to the IM. The cost function of the MP-DTC can be expressed as follows:

$$\Lambda = \left|T^*_{e,k+1} - T_{e,k+1}\right| + W_f\left|\psi^*_{s\,k+1} - \psi_{s,k+1}\right| \quad (15)$$

where $T^*_{e,k+1}$ is the reference torque, $\psi^*_{s,k+1}$ is the reference flux, $T_{e,k+1}$ is the predicted torque at instant $(K+1)T_s$ and $\psi_{s,k+1}$ is the predicted flux at instant $(K+1)T_s$. The prediction of both the stator flux and torque at instant $(K+1)T_s$ are calculated using equations (6-10). Meanwhile, the reference torque is obtained using a designed PI torque regulator. The control scheme of this MP-DTC can be constructed as shown in Figure 5.

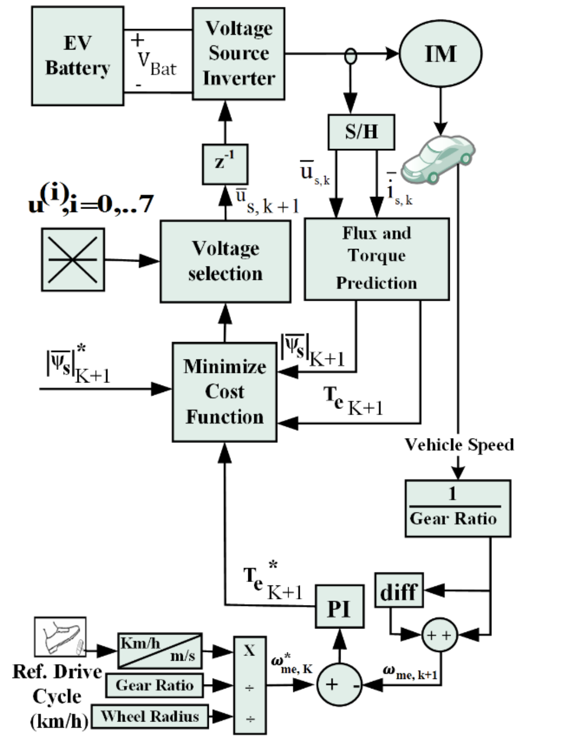

Figure 5: Block diagram of the MP-DTC for IM in an EV system

3.3. Predictive Current Control

In this subsection, the predictive current control (PCC) technique is developed to control the EV speed, and the EV's IM torque and flux. The control technique aims to maintain the stator current components ($i_{ds,k}$, and $i_{qs,k}$), which represent both the flux and the torque respectively, as near as possible to their reference values at each sampling instant. The references of both the current components are obtained based on the rotor field-oriented control technique principles as obtained by equations (11 and 12). The error vector at the time instant KT_s can be expressed by:

$$\bar{e}_k = (i^*_{ds,k} - i_{ds,k}) + j(i^*_{qs,k} - i_{qs,k}) \quad (16)$$

The PCC aims to push the error vector very near to zero by selecting the appropriate voltage vector to be applied to the IM in the next control cycle.

3.3.1. Prediction of the stator current

To predict the current value based on the Euler method, which requires obtaining the derivatives of the IM stator current components which can be expressed based on the IM model illustrated by equations (6-9):

$$\left(\frac{di_{ds}}{dt}\right)_k = \frac{l_r}{l_s l_r - l_m^2}\left[u_{ds,k} - R_s i_{ds,k} + w_s\,\frac{l_r}{l_s l_r - l_m^2}\,i_{qs,k}\right] \quad (17)$$

$$\left(\frac{di_{qs}}{dt}\right)_k = \frac{l_r}{l_s l_r - l_m^2}\left[u_{qs,k} - R_s i_{qs,k} - w_s \psi_{ds,k}\right] \quad (18)$$

The prediction of the IM stator current at instant $T_s(k+1)$ can be obtained by the following equations:

$$(i_{ds})_{k+1} = i_{ds,k} + T_s\left(\frac{di_{ds}}{dt}\right)_k \quad (19)$$

$$(i_{qs})_{k+1} = i_{qs,k} + T_s\left(\frac{di_{qs}}{dt}\right)_k \quad (20)$$

3.3.2. Selecting the optimum stator voltage vector

The optimum voltage vector that will be applied to the IM is the voltage vector that minimizes the cost function based on the error vector expressed by (16). The PCC predicts the cost function value at an instant (k+1) using the predicted values of currents.

$$\Lambda_{k+1} = \left|i^*_{ds,k+1} - i_{ds,k+1}\right| + \left|i^*_{qs,k+1} - i_{qs,k+1}\right| \quad (21)$$

The PCC scheme for the EV system is illustrated in Figure 6. The IM stator currents and voltages are measured then, the measured voltages and currents are sampled before estimating the prediction of both the direct and quadrature components of the IM stator current. The predicted current components and the reference current components are compared through the PCC cost function (21). Lastly, the cost function is minimized by selecting the appropriate voltage vector to be applied across the IM terminals.

4. EV system Testing

Using MATLAB/Simulink software tool, the complete EV system was tested to analyze the EV dynamic performance. The EV system was tested under the field-oriented control-based hysteresis current control and the predictive current control techniques. The performed tests were done under the WLTP reference drive cycle. The vehicle, IM, battery, and control parameters are illustrated in Appendix A.

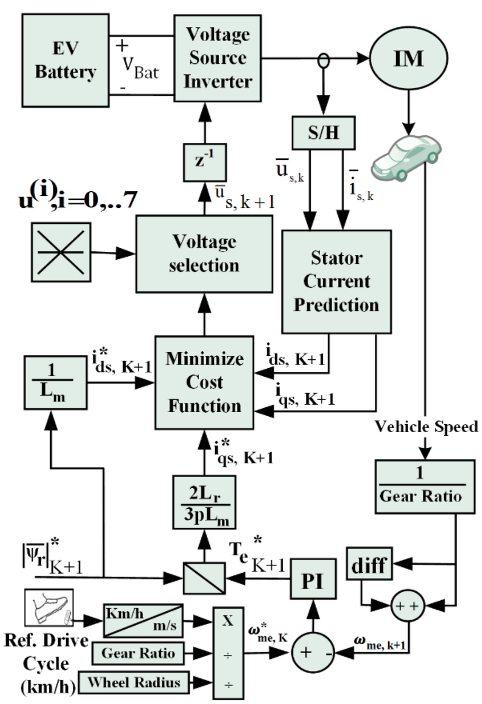

Figure 6: Block diagram of the PCC for IM in an EV system

4.1. Results under the FOC-HCC technique

In this subsection, the complete EV system was evaluated using the FOC-HCC technique. Figure 7 presents the EV speed which had speed error from the WLTP reference applied drive cycle as shown in Figure 8. The IM-developed torque as shown in Figure 9 had high torque ripples.

The IM stator flux under the FOC-HCC technique is presented in Figure 10 which reports a high ripple content. Figure 11 illustrates the three-phase currents of the IM which suffer from high current ripple. Figures 12-a, 12-b, and 12-c illustrate the FFT spectrum of the three-phase IM stator currents. The FFT analysis of the IM stator currents shows a total harmonic distortion (THD) of about 1.41%, 0.92%, and 1.46% of the fundamental values respectively. The illustrated current ripples content can be also illustrated by the loci of the stator flux illustrated in Figure 13. Figures 14 and 15 illustrate both the EV battery terminal voltage and the state of charge of the EV battery under the FOC-HCC control method.

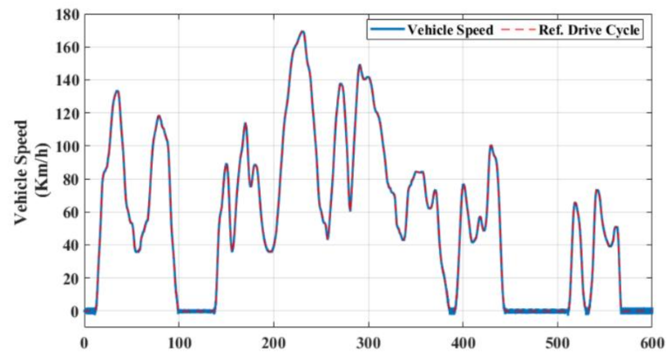

Figure 7: The EV speed based on the FOC-HCC technique

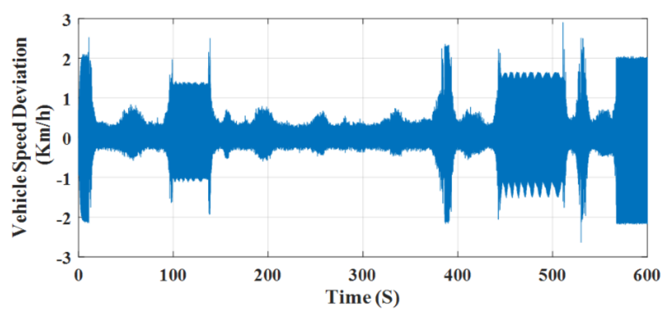

Figure 8: The deviation of EV speed from the WLTP reference under the FOC-HCC technique

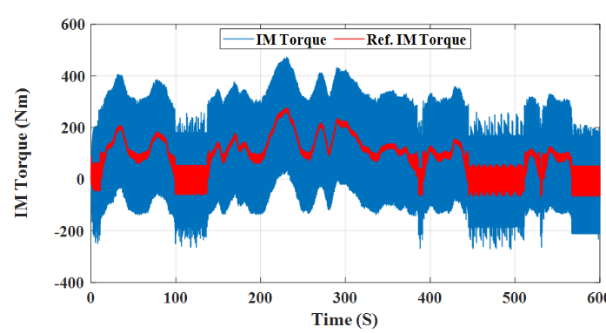

Figure 9: The IM torque under the FOC-HCC technique

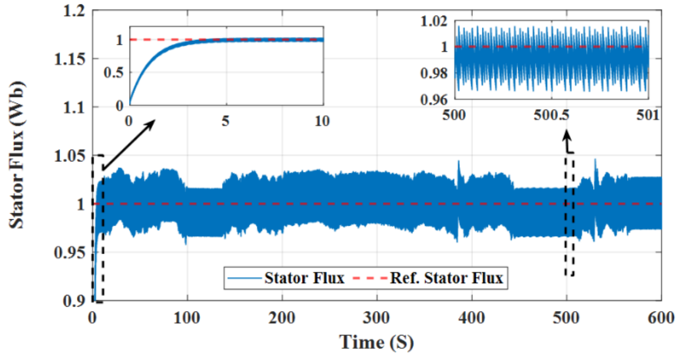

Figure 10: The IM stator flux under the FOC-HCC technique

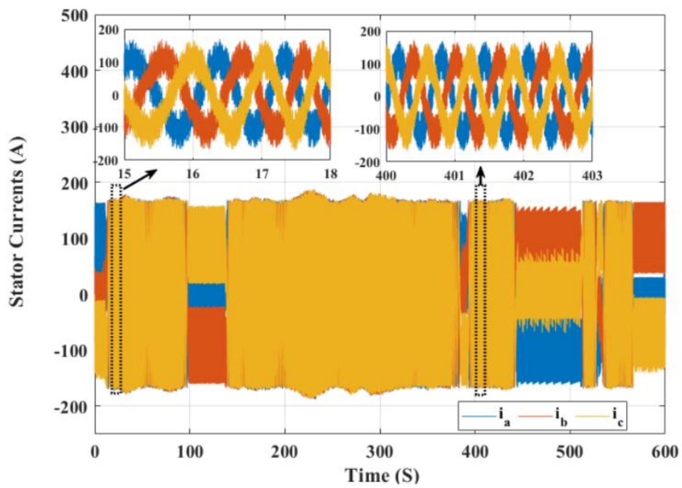

Figure 11: The IM stator currents under the FOC-HCC technique

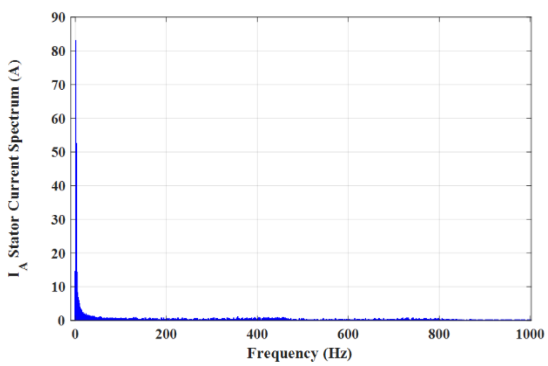

(a)

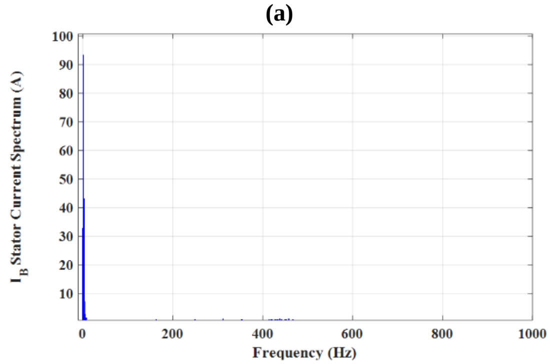

(b)

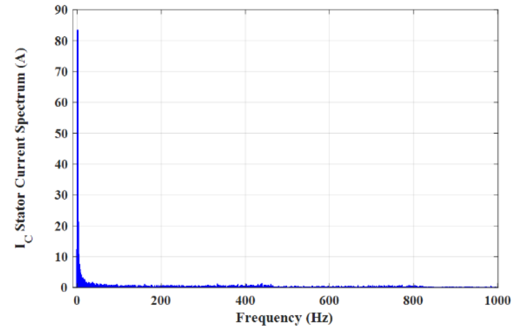

(c)

Figure 12: The IM stator currents spectrum under the FOC-HCC technique, (a) phase a current spectrum; (b) phase b current spectrum; (c) phase c current spectrum

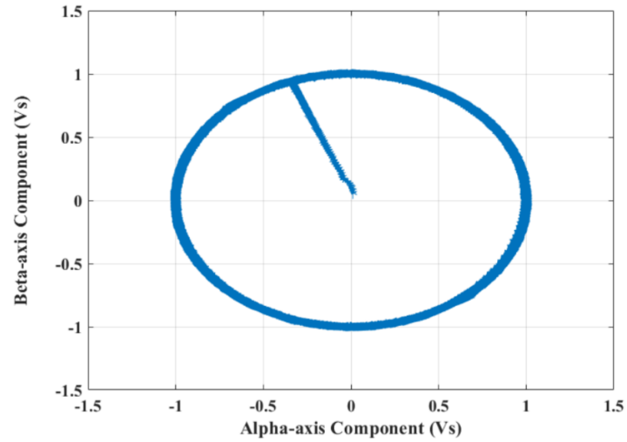

Figure 13: The IM stator flux loci under the FOC-HCC technique

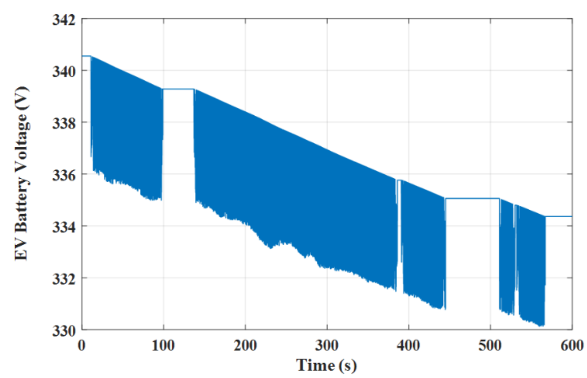

Figure 14: The terminal voltage across the EV battery under the FOC-HCC technique

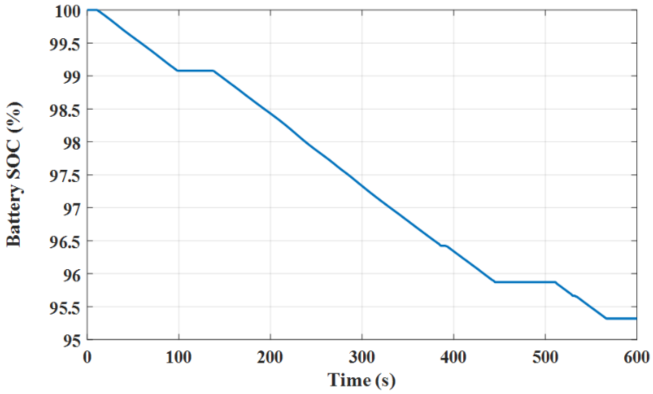

Figure 15: The EV battery state of charge under the FOC-HCC technique

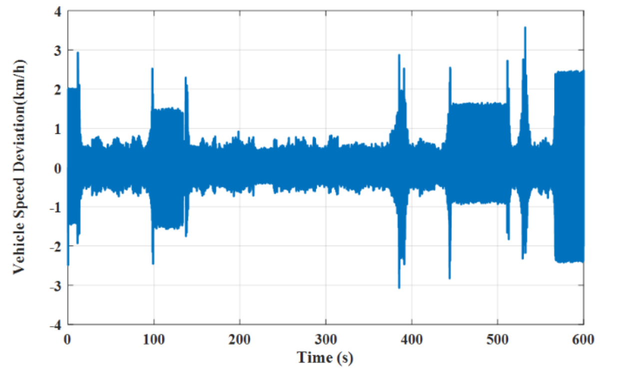

Figure 17: The EV speed deviation under the MP-DTC technique

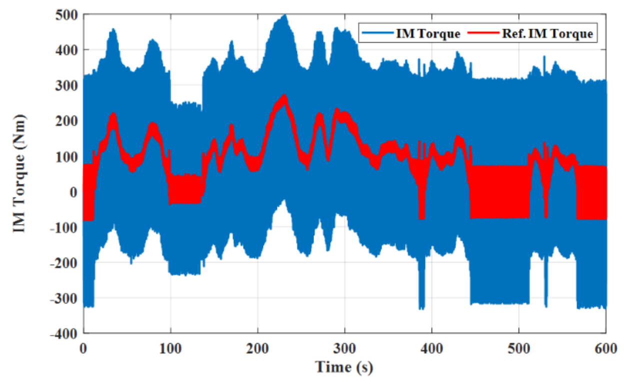

Figure 18: The IM torque under the MP-DTC technique

4.2. Results under the MP-DTC technique

In this subsection, the complete EV system was evaluated using the MP-DTC technique. Figure 16 presents the EV speed which had speed error from the WLTP reference applied drive cycle as shown in Figure 17. The IM-developed torque as shown in Figure 18 had high torque ripples compared with that obtained under the FOC-HCC.

The IM stator flux under the MP-DTC technique is presented in Figure 19 which illustrates a high ripple content. Figure 20 illustrates the three-phase currents of the IM which suffer from high current ripple. Figures 21-a, 21-b, and 21-c illustrate the FFT spectrum of the three-phase IM stator currents. The FFT analysis of the IM stator currents shows a total harmonic distortion (THD) of about 2.32%, 1.26%, and 1.53% of the fundamental values respectively. The illustrated current ripples content can be also illustrated by the loci of the stator flux illustrated in Figure 22. Figures 23 and 24 illustrate both the EV battery terminal voltage and the state of charge of the EV battery under the MP-DTC control method.

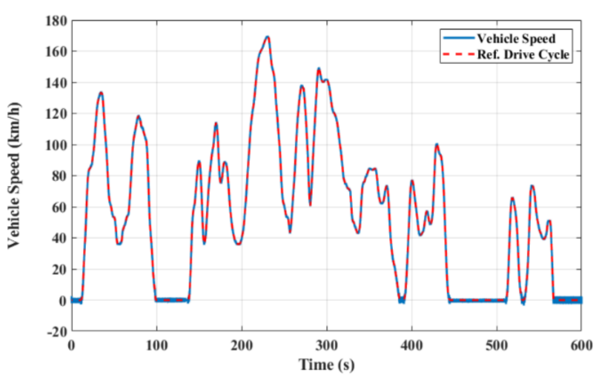

Figure 16: The EV speed under MP-DTC technique

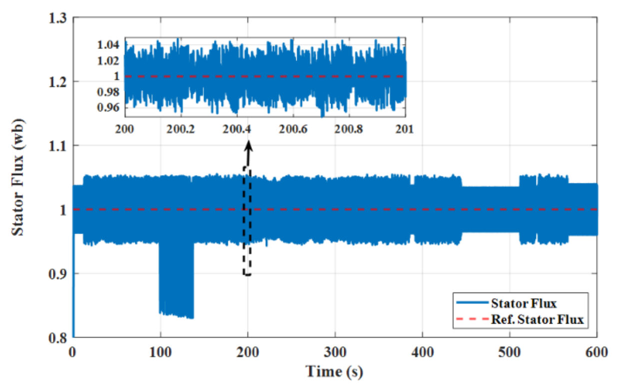

Figure 19: The IM stator flux under the MP-DTC technique

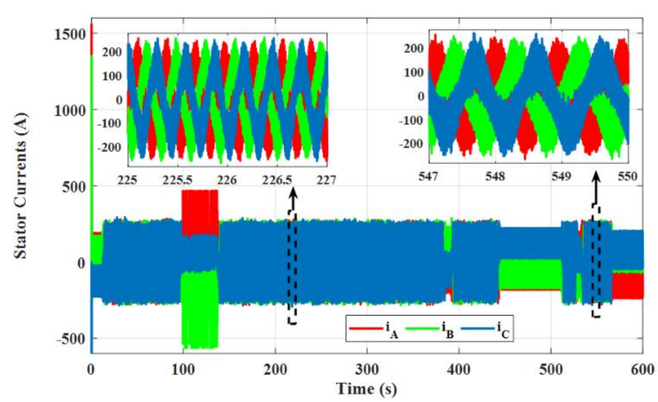

Figure 20: The IM stator currents under the MP-DTC technique

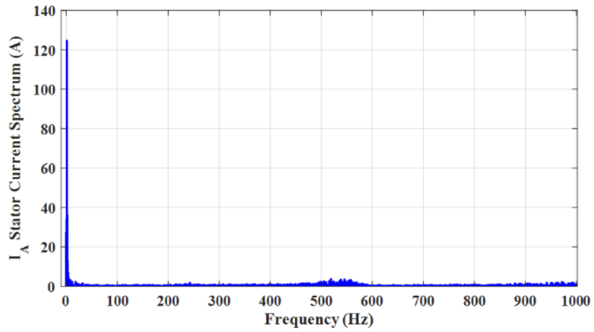

(a)

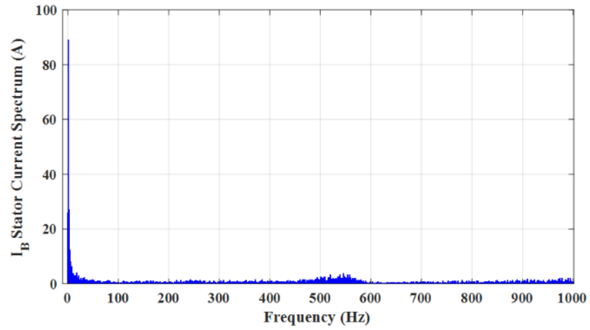

(b)

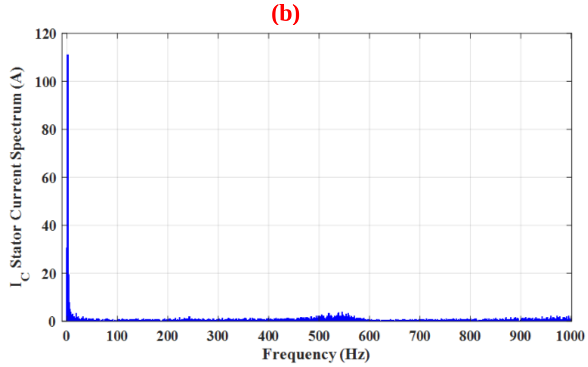

(c)

Figure 21: The IM stator currents spectrum under the MP-DTC technique, (a) phase a current spectrum; (b) phase b current spectrum; (c) phase c current spectrum

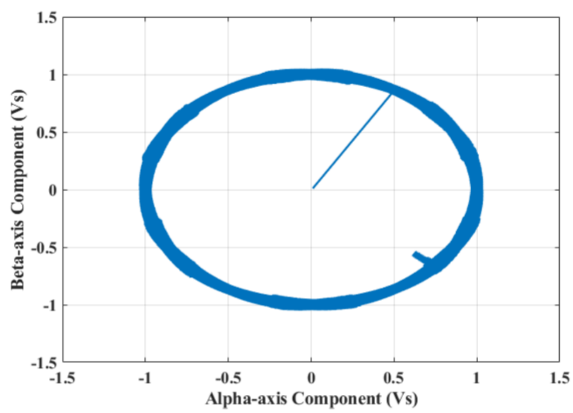

Figure 22: The stator flux loci under the MP-DTC technique

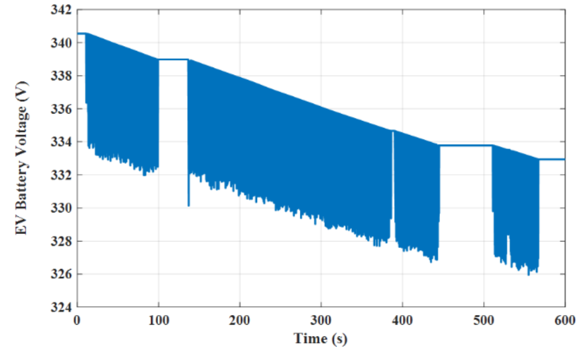

Figure 23: The EV battery terminal voltage under the MP-DTC technique

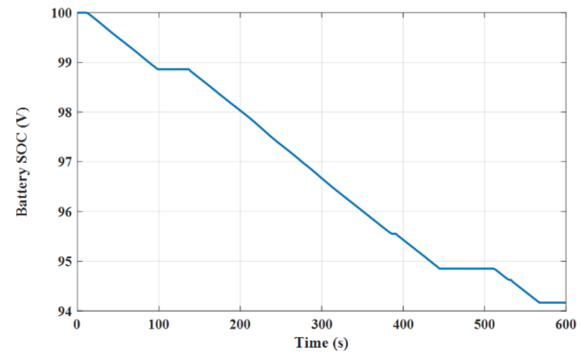

Figure 24: The EV battery state of charge under the MP-DTC technique

4.3. Results under the PCC technique

In this subsection, the EV system was tested under the predictive current control technique. Figure 25 presents the speed of the EV under the PCC technique. The EV speed deviation from the reference drive cycle (WLTP) is shown in Figure 26. The IM-developed torque under the PCC is illustrated in Figure 27. The IM torque has a small ripple content under PCC compared with the results obtained under the other control techniques. Figure 28 shows the IM stator flux under the PCC technique.

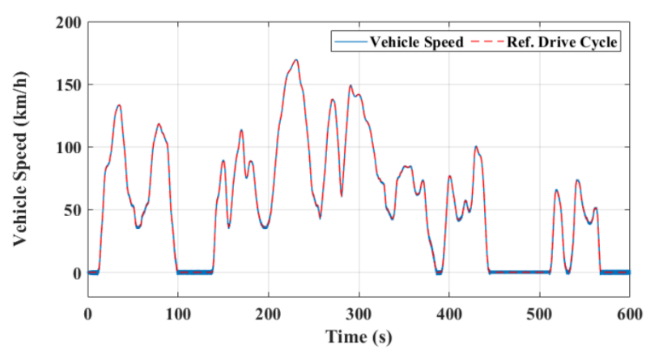

Figure 25: The EV Speed under the PCC technique

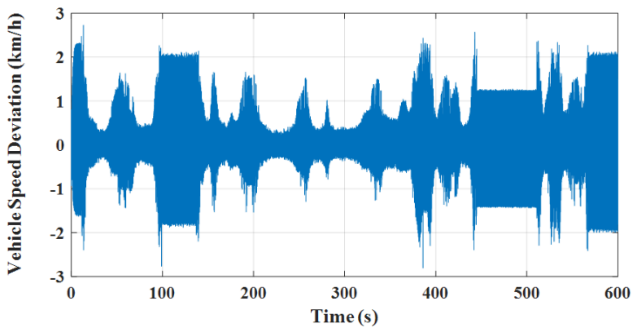

Figure 26: The deviation of EV speed from the WLTP reference under the PCC technique

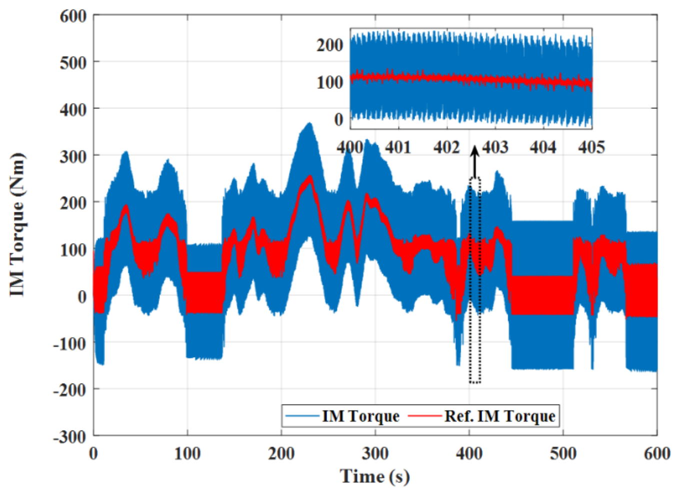

Figure 27: The IM developed torque under the PCC technique

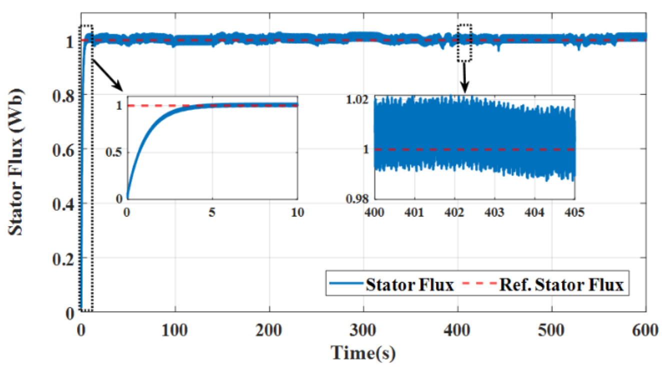

Figure 28: The IM stator under the PCC technique

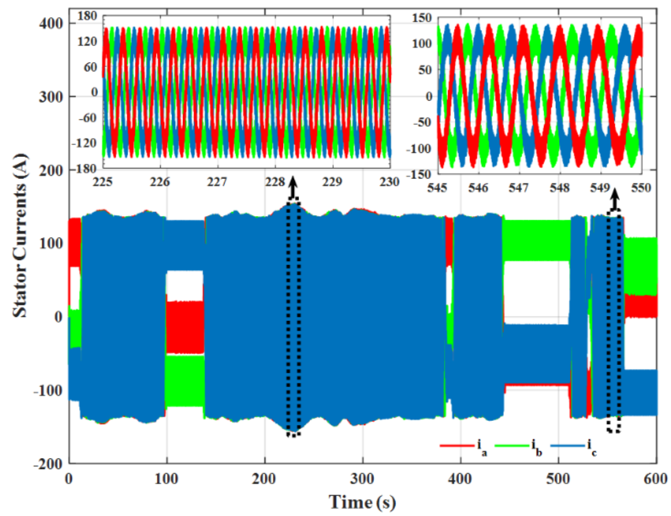

Figure 29: The three-phase stator currents under the PCC technique

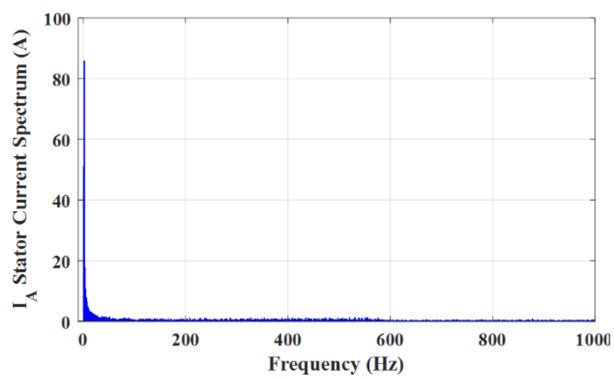

Figure 30: (a)

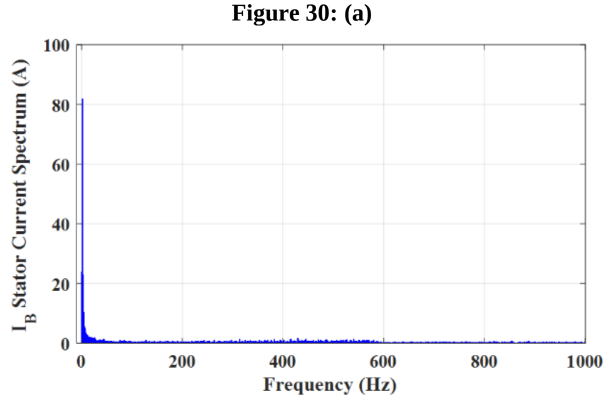

(b)

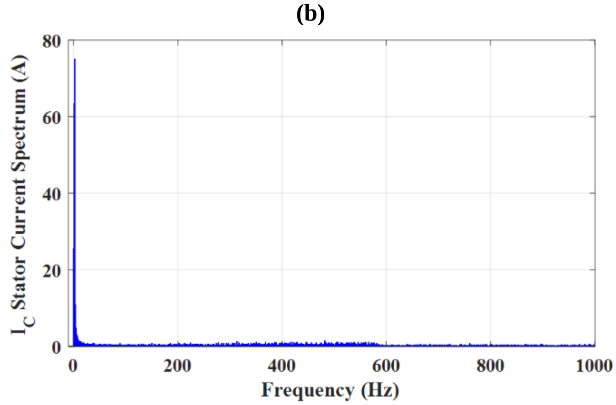

(c)

Figure 29 illustrates the three-phase stator currents under the PCC techniques. Figures 30-a, 30-b and 30-c show the FFT spectrum analysis of the stator currents which report a THD of about 0.98%, 0.8%, and 0.65% of the fundamental values. The IM stator currents have the smallest current ripple content compared to that observed under the other control techniques. Figure 31 presents the loci of the stator flux. Figures 32 and 33 illustrate both the terminal voltage across the EV battery and the state of charge of the EV battery under the PCC.

Figure 30: The IM stator currents spectrum under the PCC technique, (a) current spectrum of phase a; (b) current spectrum of phase b; (c) current spectrum of phase c.

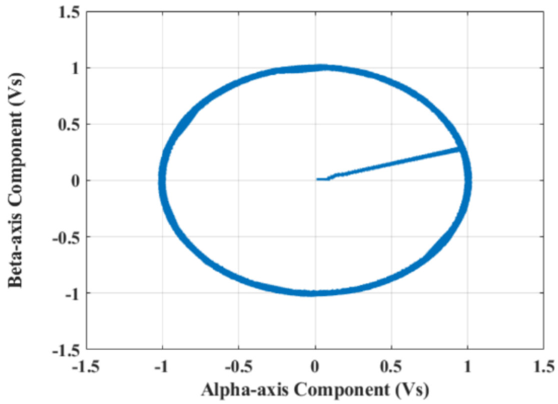

Figure 31: The stator flux loci under the PCC technique

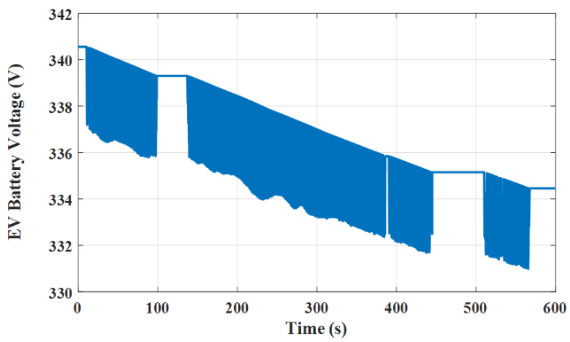

Figure 32: The terminal voltage across the EV battery under the PCC technique

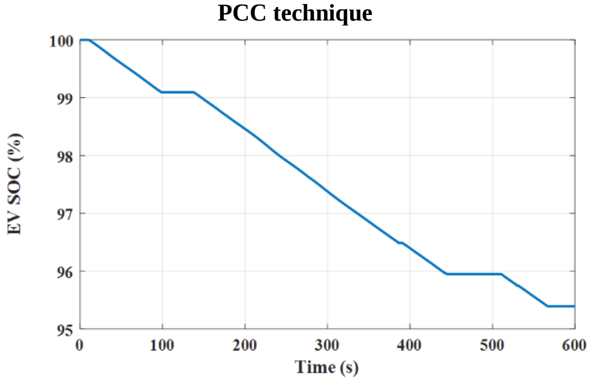

Figure 33: The EV battery state of charge under the PCC technique

4.4. Comparison between the FOC-HCC and the PCC techniques

To select the best control technique, a comparative study between the EV performance under both the three control techniques. Figure 34 illustrates the IM torque under both techniques which presents a small torque ripple under PCC compared to that obtained under the other control techniques. Figure 35 shows the IM stator flux of the IM which indicates a small ripple content under the PCC compared to that obtained under the other control techniques. The aberration of both the IM stator flux developed torque modulus from their references were taken also as a measure of a controller primacy compared to the other and this is presented in Table 1 which shows that the PCC has minimum IM torque and stator flux ripples compared to the other control methods.

Table 1: IM torque and stator flux ripples

	MP-DTC	FOC-HCC	PCC
IM toque ripple	89.4%	81.6%	38.3%
Stator flux ripple	±14.8%	±4.6%	±3.34%

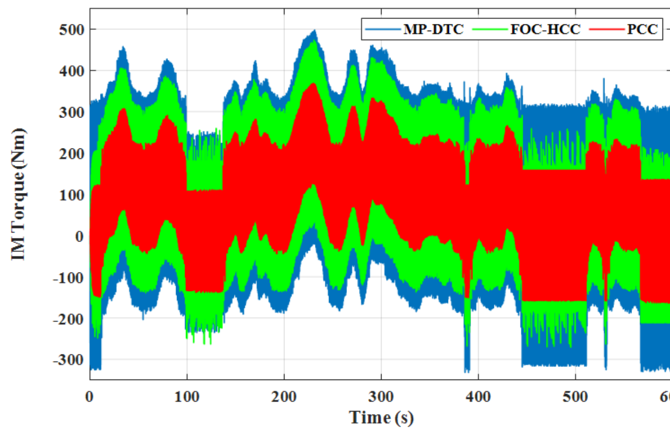

Figure 34: The IM developed torque under both the FOC-HCC and the PCC technique

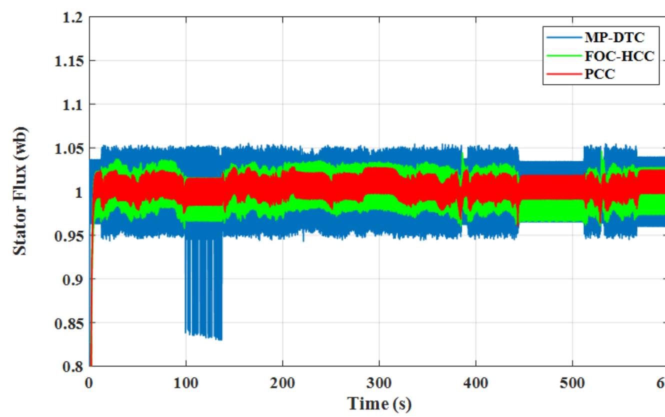

Figure 35: The IM stator flux under both the FOC-HCC and the PCC technique

Comparing the THD values of the three-phase stator currents as illustrated in Table 2. It can be observed that the PCC control technique had a smaller THD for the stator currents compared to that obtained under the other control methods. The superiority of the PCC technique over both the MP-DTC and the FOC-HCC technique can also be verified by the loci of the stator flux illustrated in Figure 36.

Figure 37 illustrates the smaller EV battery terminal voltage variation under PCC compared to both the MP-DTC and the FOC-HCC. Also, the EV battery state of charge is larger under the PCC compared to the other control techniques as presented in Figure 38 which presented a low battery discharge rate under the PCC which permits the vehicle to travel a long distance under the PCC technique compared to the other control techniques.

Table 2: The stator currents THD under both the FOC-HCC and PCC techniques

	MP-DTC	FOC-HCC	PCC
THD of IM stator current phase A (% of the fundamental)	2.32%	1.41%	0.98%
THD of IM stator current phase B (% of the fundamental)	1.26%	0.92%	0.8%
THD of IM stator current phase C (% of the fundamental)	1.53%	1.46%	0.65%

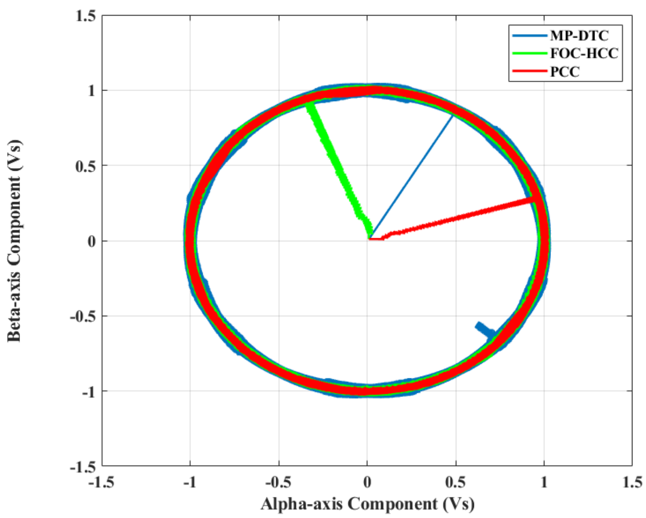

Figure 36: The loci of the IM stator flux under both the FOC-HCC and the PCC technique

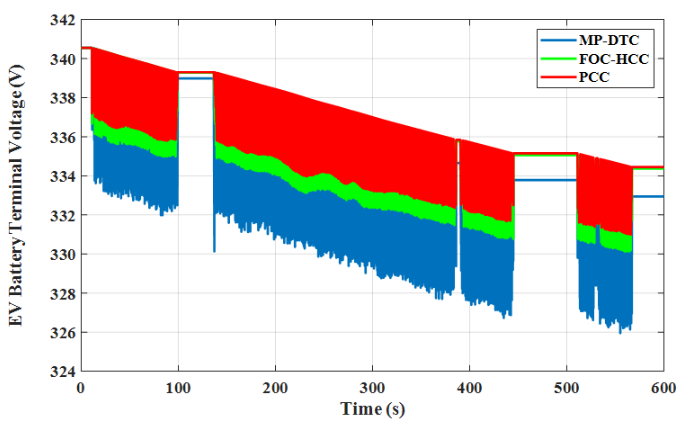

Figure 37: The EV battery terminal voltage under both the FOC-HCC and the PCC technique

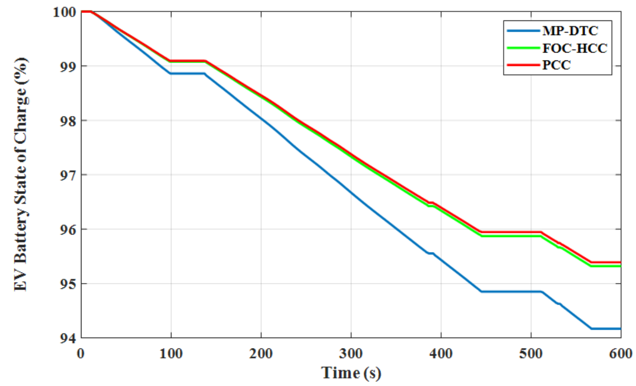

Figure 38: The EV battery state of charge under both the FOC-HCC and the PCC technique

5. Conclusions

This article introduced the EV system modeling as a first step to studying its dynamic performance. Three different control methods were introduced and developed to control the EV system. The EV dynamic performance was tested under FOC-HCC, MP-DTC and PCC techniques. The observed results prove that the PCC has superiority over the other control techniques. Finally, the following points can be elaborated:

- The EV system model was introduced.
- The theoretical base of the FOC-HCC, MP-DTC and the PCC were presented and applied to control the complete EV system.
- A comparative study of the EV system performance under FOC-HCC, MP-DTC and PCC was presented.
- The advantages of the PCC compared to the other control techniques are illustrated as lower torque ripple content, small flux ripples, lower stator currents THD, smaller EV battery terminal voltage variation, and lower EV battery discharging.

Appendix A

The parameters of the EV system are presented in Table A1.

Table A1: EV system Parameters

Parameter	Value
Vehicle parameters	
Vehicle's mass	1645 kg
EV wheel radius	31.5 cm
Air density	1.225 kg/m^3
Road rolling resistance coefficient	0.0083
Gravity acceleration	9.81 m/s^2
Aerodynamic drag coefficient	0.46
Gear ratio	10
Gear efficiency	96%
Wind speed	10 m/s
EV front area	3 m^2
Coefficient of bearing fraction	0.001
Hill slope angle	5 deg
IM parameters	
Induction Motor Rated Power	160 kW
Line voltage	400 V
Supply Frequency	50 Hz
Number of Pole pairs	2
Rated speed	1487 rpm
Nominal torque	1027 N.m

Nominal flux	**1 wb**
IM Inertia J	**2.9 kg.m^2**
R_s	**0.01379 Ω**
L_s	**7.842 mH**
R_r	**0.007728 Ω**
L_r	**7.842 mH**
L_m	**7.69 mH**
EV battery parameters	
Battery constant voltage	**280 V**
Battery polarization constant	**0.05 V**
The capacity of the EV Battery	**50 Ah**
EV Battery exponential zone amplitude	**60.6 V**
Time constant inverse of the battery exponential zone	$\mathbf{0.046\ (Ah)^{-1}}$
The internal resistance of the EV battery	**0.097 Ω**
Controller's Parameters	
Sampling period	**100μs**
Proportional gain (K_P) of the IM speed controller	**257.6**
integral gain (K_I) of the IM Speed controller	**22890**
IM Reference (Nominal) flux	**1 wb**
Limits of IM torque	$\pm$**1027 Nm**

References

[1] C. C. Chan, A. Bouscayrol, and K. Chen, "Electric, Hybrid, and Fuel-Cell Vehicles: Architectures and Modeling," *IEEE Transactions on Vehicular Technology*, vol. 59, no. 2, pp. 589-598, 2010.

[2] W. Xu, J. Zhu, Y. Guo, S. Wang, Y. Wang, and Z. Shi, "Survey on electrical machines in electrical vehicles," in *2009 International Conference on Applied Superconductivity and Electromagnetic Devices*, 2009, pp. 167-170.

[3] S. Sharifan, S. Ebrahimi, A. Oraee, and H. Oraee, "Performance comparison between brushless PM and induction motors for hybrid electric vehicle applications," in *2015 Intl Aegean Conference on Electrical Machines & Power Electronics (ACEMP), 2015 Intl Conference on Optimization of Electrical & Electronic Equipment (OPTIM) & 2015 Intl Symposium on Advanced Electromechanical Motion Systems (ELECTROMOTION)*, 2015, pp. 719-724.

[4] D. Çelik and M. E. Meral, "A coordinated virtual impedance control scheme for three phase four leg inverters of electric vehicle to grid (V2G)," *Energy,* vol. 246, p. 123354, 2022/05/01/ 2022.

[5] H. Ahmed and D. Çelik, "Sliding mode based adaptive linear neuron proportional resonant control of Vienna rectifier for performance improvement of electric vehicle charging system," *Journal of Power Sources,* vol. 542, p. 231788, 2022/09/15/ 2022.

[6] D. Çelik, "Lyapunov based harmonic compensation and charging with three phase shunt active power filter in electrical vehicle applications," *International Journal of Electrical Power & Energy Systems,* vol. 136, p. 107564, 2022/03/01/ 2022.

[7] M. A. Mossa and S. Bolognani, "Effective sensorless Direct Torque Control for an induction motor drive with reduced ripple contents," in *2016 IEEE International Conference on Power Electronics, Drives and Energy Systems (PEDES)*, 2016, pp. 1-6.

[8] A. Haddoun, M. Benbouzid, D. Diallo, R. Abdessemed, J. Ghouili, and K. Srairi, "Comparative analysis of control techniques for efficiency improvement in electric vehicles," in *2007 IEEE Vehicle Power and Propulsion Conference*, 2007, pp. 629-634: IEEE.

[9] Q. Tang, X. Ge, Y.-C. Liu, and M. Hou, "Improved switching-table-based DTC strategy for the post-fault three-level NPC inverter-fed induction motor drives," *IET Electric Power Applications,* vol. 12, no. 1, pp. 71-80, 2018/01/01 2018.

[10] B. Singh, P. Jain, A. Mittal, and J. Gupta, "Speed sensorless electric vehicle propulsion system using DTC IM drive," in *2006 India International Conference on Power Electronics*, 2006, pp. 7-11: IEEE.

[11] W. Qinglong, Y. Changzhou, and Y. Shuying, "Indirect Field Oriented Control Technology for Asynchronous Motor of Electric Vehicle," in *2020 IEEE International Conference on Power, Intelligent Computing and Systems (ICPICS)*, 2020, pp. 673-677.

[12] Y. Wang and K. Zhao, "Field-oriented vector control of induction motor for electric vehicles," in *31st Annual Conference of IEEE Industrial Electronics Society, 2005. IECON 2005.*, 2005, p. 5 pp.

[13] J. Zhang, L. Li, L. Zhang, and D. G. Dorrell, "Hysteresis band current controller based field-oriented control for an induction motor driven by a direct matrix converter," in *IECON 2017 - 43rd Annual Conference of the IEEE Industrial Electronics Society*, 2017, pp. 4633-4638.

[14] M. A. Mossa and S. Bolognani, "Model Predictive Phase Angle Control for an Induction Motor Drive," in *2018 Twentieth International Middle East Power Systems Conference (MEPCON)*, 2018, pp. 128-134.

[15] M. A. Mossa and S. Bolognani, "Implicit predictive flux control for high-performance induction motor drives," *Electrical Engineering,* vol. 103, no. 1, pp. 373-395, 2021/02/01 2021.

[16] M. A. Mossa, M. K. Abdelhamid, A. A. Hassan, and N. Bianchi, "Improving the Dynamic Performance of a Variable Speed DFIG for Energy Conversion Purposes Using an Effective Control System," *Processes,* vol. 10, no. 3, 2022.

[17] M. A. Mossa, "Effective predictive current control for a sensorless five-phase induction motor drive," *International Journal of Power Electronics,* vol. 13, no. 4, pp. 502-532, 2021/01/01 2021.

[18] M. A. Mossa and S. Bolognani, "Robust Predictive Current Control for a Sensorless IM Drive Based on Torque Angle Regulation," in *2019 IEEE Conference on Power Electronics and Renewable Energy (CPERE)*, 2019, pp. 302-308.

[19] M. A. Mossa and S. Bolognani, "Effective model predictive current control for a sensorless IM drive," in *2017 IEEE International Symposium on Sensorless Control for Electrical Drives (SLED)*, 2017, pp. 37-42.

[20] M. A. Mossa, O. M. Kamel, and S. Bolognani, "Explicit Predictive Voltage Control for an Induction Motor Drive," in *2019 21st International Middle East Power Systems Conference (MEPCON)*, 2019, pp. 258-264.

[21] H. Echeikh, M. A. Mossa, N. V. Quynh, A. A. Ahmed, and H. H. Alhelou, "Enhancement of Induction Motor Dynamics Using a Novel Sensorless Predictive Control Algorithm," *Energies,* vol. 14, no. 14, 2021.

[22] J. Kang, X. Li, Y. Liu, S. Mu, and S. Wang, "Predictive Current Control with Torque Ripple Minimization for PMSM of Electric Vehicles," in *2018 IEEE International Power Electronics and Application Conference and Exposition (PEAC)*, 2018, pp. 1-6.

[23] M. R. M. Hassan, M. A. Mossa, and G. M. Dousoky, "Evaluation of Electric Dynamic Performance of an Electric Vehicle System Using Different Control Techniques," *Electronics,* vol. 10, no. 21, 2021.

[24] M. Ehsani, Y. Gao, S. Longo, and K. Ebrahimi, *Modern electric, hybrid electric, and fuel cell vehicles*. CRC press, 2018.

[25] L. S and L. P. P.S, "Mathematical modeling of Electric vehicles - A survey," *Control Engineering Practice,* vol. 92, p. 104138, 2019/11/01/ 2019.

[26] H. Abu-Rub, A. Iqbal, and J. Guzinski, *High performance control of AC drives with MATLAB/Simulink models*. John Wiley & Sons, 2012.

[27] A. M. Trzynadlowski, "4 - Power electronic converters for induction motor drives," in *Control of Induction Motors*, A. M. Trzynadlowski, Ed. San Diego: Academic Press, 2001, pp. 55-92.

[28] H. M. Soliman and S. Hakim, "Improved Hysteresis Current Controller to Drive Permanent Magnet Synchronous Motors through the Field Oriented Control," *International Journal of Soft Computing Engineering,* vol. 2, no. 4, pp. 343-346, 2012.

[29] M. Mamdouh and M. A. Abido, "Efficient Predictive Torque Control for Induction Motor Drive," *IEEE Transactions on Industrial Electronics,* vol. 66, no. 9, pp. 6757-6767, 2019.